Available online at www.sciencedirect.com
SCIENCE DIRECT®

Journal of the European Ceramic Society 24 (2004) 2389–2397
www.elsevier.com/locate/jeurceramsoc

Phase transformation and growth of mullite in kaolin ceramics

Yung-Feng Chen[a,*], Moo-Chin Wang[b], Min-Hsiung Hon[a]

[a]*Department of Materials Science and Engineering, National Cheng Kung University, 1 Ta-Hsueh Road, Tainan 70101, Taiwan*
[b]*Department of Mechanical Engineering, National Kaohsiung University of Applied Sciences, 415 Chien-Kung Road, Kaohsiung 80782, Taiwan*

Received 10 February 2003; received in revised form 11 June 2003; accepted 22 June 2003

Abstract

The phase transformation and growth of mullite ($3Al_2O_3{\cdot}2SiO_2$) in kaolin ceramics have been investigated using X-ray diffractometer, transmission electron microscope, select area electron diffractometer, energy dispersion spectrometer and differential thermal analysis. The mullite which was transformed from kaolin appears at 1050 °C by XRD and tallies with DTA. The initial mullite crystal showed a plate-like morphology. The Al_2O_3 content in mullite crystal increased from 49.57 to 71.37 wt.% but the lattice parameters of *a*, *b* and *c* axes decreased from 8.085, 8.106 and 3.215 Å to 7.882, 7.974 and 2.946 Å, respectively, with the grain width increasing from 20 to 70 nm when the kaolin was sintered at 1300 °C for 30 min. The nonisothermal activation energy of mullite crystallization in kaolin ceramics was 1182.3 kJ mol^{-1}. The growth morphology parameters *n* and *m* were both about 2.0, indicating that the bulk nucleation was dominant in mullitization and the crystal growth was controlled by diffusion. Seemingly, this study has been attempted to provide an integrative presentation of the thermal–structural characterization together with detailed kinetic and mechanistic interpretations.

Keywords: Grain growth; Kaolin; Mullite; Phase transformation

1. Introduction

''Kaolin'' is a major raw material for the fabrication of conventional ceramics. It occurs as an alteration product of the granitoid rocks and consists of mostly kaolinite, ideally given as $Al_2Si_2O_5(OH)_4$, and minor amounts of impurities as micas, other phyllosilicates, iron/titanium oxides and quartz.[1] While kaolin may be considered to be well studied in the past decades for serving the conventional ceramics; however, there have been renewed interests in the conversion of kaolin to mullite ($3Al_2O_3{\cdot}2SiO_2$) for the purpose of further understanding in the preparation of technical ceramics, in particular, as porous materials for filtration and structural ceramics having both high strength and thermal stability.

The rapidly advancing capabilities of characterization by highly resolving precision apparatus seems to have prompted the publication of high significant new data related to the structural transformation of kaolinite to mullite. For example, Friemann and Rahmsn[2] have vividly presented the X-ray diffraction patterns of 2:1 and 3:2 mullite and through a 2D/3D video-graphic procedure has provided indispensable graphic information on the diffuse scattering phenomena. A more comprehensive integration of the general characterization of the thermal–structural relationship together with the kinetic and mechanistic interpretations are considered to be both desirable and formidable, albeit requiring tedious efforts. In cognizance, this study has attempted to tackle such a task undertaking.

The phase transformation of sintered kaolinite has been observed by Brindley et al.[3–5] They were first set-out to settle the controversy with considerable success, at least for the clay minerals. In their opinion, the dominant feature of the entire kaolinite–mullite series is the structural continuity and especially the maintenance of essentially close-packed oxygen layers as the metakaolinite ($Al_2O_3{\cdot}2SiO_2$) as fired at 900–1000 °C, and then the Al–Si spinel they claimed of gamma alumina with silica in solid solution with the composition of $Si_3Al_4O_{12}$. Both of metakaolin and Al–Si spinel phases are shown in short range order in crystal structure. When heated above 1000 °C, the mullite begins to crystallize and has preferred orientation with the *c* axis parallel to <110> of the Al–Si spinel phase.

* Corresponding author. Fax.: +886-6-238-0208.
E-mail address: Feng@cubic.mat.ncku.edu.tw (Y.-F. Chen).

0955-2219/$ - see front matter © 2003 Elsevier Ltd. All rights reserved.
doi:10.1016/S0955-2219(03)00631-9

Various raw materials and preparation methods have been investigated for sintered mullite, fused-mullite[6,7] and chemical-mullite. The kinetics and mechanism of phase transformation of kaolinite[3–11] or Al_2O_3–SiO_2 raw materials[12–15] have been investigated by isothermal [8–11,15] or nonisothermal method,[12,14,16,17] and the related problem of the structural modifications occurs [10,11,13,15] during the raw materials transit to metakaolinite, Al–Si spinel and mullite. The nucleation and growth phenomena of mullite from more ordered kaolinite proceeding at lower temperatures than from disordered kaolinite may be an evidence for preservation of the aluminum oxygen octahedra chains of the Al–Si spinel phase during mullite formation in the case of ordered kaolinite starting material. [13,15] The activation energies of mullite nucleation and growth were found to relate with the defective structure of the starting kaolinite, which thus must have an influence on the chemical homogeneity of the intermediate phase. The initial reaction mechanism affected the mullite nucleation; subsequently the reaction process shifted toward a grain growth-limited process that was intermediate between phase boundary and diffusion controlled.[8] However, the crystallization kinetics and growth mechanism of mullite formation in kaolin have not been studied in detail.

In the present integrative study, the crystallization kinetics and growth mechanism of mullite formation in kaolin were studied using X-ray diffractometer (XRD), transmission electron microscope (TEM), select area electron diffractometer (SAED), energy dispersion spectrometer (EDS) and differential thermal analysis (DTA). The purposes of this investigation are to (i) study the mullite transformation in kaolin, (ii) investigate the mullite crystal morphology and structure by TEM, (iii) estimate the activation energy of mullite formation based on a nonisothermal method and (iv) demonstrate the growth mechanism of mullite.

2. Experimental procedure

2.1. Sample preparation

The raw material powders of kaolin were supplied by Associated Kaolin Industries Berhad (AKIMA-25, Ipoh, Malaysia, average size 1.3 μm) with the chemical compositions was listed in Table 1. All specimens were derived from starting powders to which a 32.4 wt.% multiple-organics solution as binder consisting of 16.6 wt.% PEG-10k, 4.2 wt.% glycerin, 25.0 wt.% selosol 920, 4.2 wt.% Celuna D-305 and 50.0 wt.% deionized water was added. The raw material powders were first blended for 60 min in a laboratory mixer. A batch (1.0 kg) of admixed raw materials with multiple-organics solution was mixed by using a double-Z blade at 25 °C for 30 min; subsequently the resulting feedstock were extrusion molded at 18 MPa using a single-screw extruder at a temperature of 25 °C to obtain a pipe sample with dimensions of radius, thickness and length of 3, 0.5 and 10 cm, respectively.

Table 1
Chemical composition of kaolin powders

Chemical composition (wt.%)	Kaolin
SiO_2	54.0
Al_2O_3	32.0
Fe_2O_3	0.98
Na_2O	0.25
TiO_2	0.45
CaO	0.06
K_2O	1.65
MgO	0.30
L.O.I.	13.1

In the thermal debinding, the water constituent was preferentially removed at 110 °C for 30 min. Glycerin, selosol 920 and celuna D-305 were extracted at about 170 °C for 60 min. The samples were then heated to 475 °C at a heating rate of 1 °C min^{-1} and held for 30 min for PEG-10k debinding. Finally, the debinded samples were sintered at 950–1400 °C for various durations at a heating rate of 5 °C min^{-1}.

2.2. Sample characterization

The phases of the sintered kaolin ceramics were identified using an X-ray diffractometer with Cu K_α radiation and a Ni filter, operated at 30 kV, 20 mA and a scanning rate of 0.25° min^{-1} (model XD-D1, Shimadzu, Kyoto, Japan).

The foil for TEM observation was prepared by slicing to a thickness of about 30 μm mechanically and ion-beam thinning to electron transparency. The morphology of the sintered samples and the chemical compositions of mullite phase were observed by TEM (Hitachi model HF-2000 Field Emission Transmission Electron Microscope, Hitachi Ltd., Tokyo, Japan, operated at 200 kV) and EDS (Noran model Voyager1000, Noran Instruments, CA, USA). The mullite crystal structure was investigated by SAED based on TEM.

DTA was conducted in the temperature range of 25–1400 °C in static air. The 200 mg raw material powders of kaolin were heated at rates of 10, 20, 30 and 40 °C min^{-1}, respectively by the Setaram TG/DTA 92 (Setaram, Caluire, France) thermal analysis system, in which Al_2O_3 powder was used as the reference material.

3. Results and discussion

3.1. Mullite phase transformation in kaolin

Fig. 1 shows the XRD patterns of the kaolin ceramics as heated at various temperatures and durations. It is found that the minor phase of quartz and mica can be

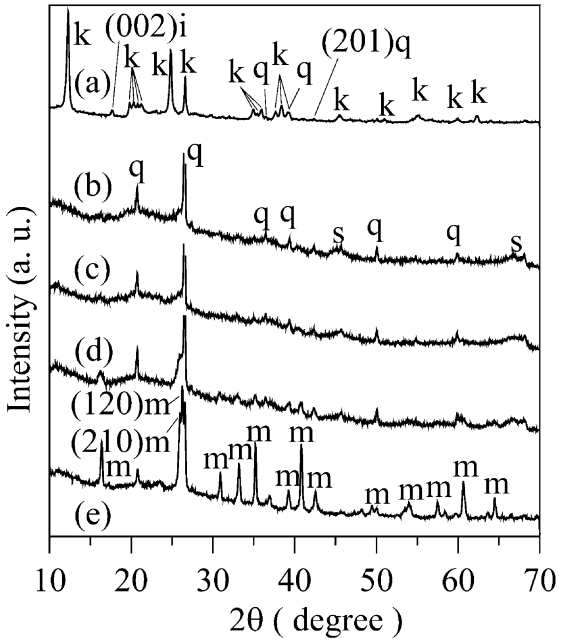

Fig. 1. XRD patterns for (a) raw material of kaolin and when the samples were sintered at (b) 950, (c) 1000, (d) 1050 °C for 24 h and (e) 1300 °C for 30 min (k: kaolinite, q: quartz, i: mica, s: Al–Si spinel and m: mullite).

detected by the reflections of (201) and (002) at $2\theta = 45.80$ and 17.61° in the unfired kaolin, respectively, by Fig. 1(a). When the samples were heated at 950 and 1000 °C for 24 h, the quartz and Al–Si spinel have been noted to be the major phases as shown in Fig. 1(b) and (c). The mullite phase appears as the sample is heated at 1050 °C for 24 h as shown in Fig. 1(d). When firing temperatures have been elevated to between 1050 and 1300 °C, the intensity increases and the much shaper X-ray reflections of mullite are observed as shown in Fig. 1(d) and (e), indicating further development of mullite formation. On the other hand, it is also found that the (120) and (210) reflections split ($2\theta = 25.97$ and 26.27°, respectively), corresponding to the result of Li et al.[18]

In consultation with the reports of Brindley and Nakahira,[3–5] when the sample is heated up to 1050 °C, the transformation from kaolinite to mullite can be explained by the following reactions in this study:

$$Al_2O_3{\cdot}2SiO_2 \cdot 2H_2O(\text{kaolinite}) \xrightarrow{400\sim500^\circ C} Al_2O_3{\cdot}2SiO_2(\text{metakaolinite}) + 2H_2O \quad (1)$$

$$2(Al_2O_3{\cdot}2SiO_2)(\text{metakaolinite}) \xrightarrow{\sim950^\circ C} Si_3Al_4O_{12}(Al-Si-\text{spinel}) + SiO_2(\text{amorphous}) \quad (2)$$

$$3Si_3Al_4O_{12}(Al-Si\ \text{spinel}) \xrightarrow{>1050^\circ C} 2(3Al_2O_3{\cdot}2SiO_2)(\text{mullite}) + 5\ \ SiO_2(\text{amorphous}) \quad (3)$$

When the kaolinite is heated, the adsorbed water is liberated at above 100 °C and the weakest part of the chemical bond is broke or perturbed; then dehydroxylation takes place at 400–500 °C. For kaolinite, dehydroxylation might result in the disturbance of the $Al(O,OH)_6$ octahedral sheet by the outer hydroxyls,[1] but does not have much effect on the SiO_4 tetrahedral sheet due to the more stable inner hydroxyls groups. The outer hydroxyls of octahedral sheets may be more easily removed by heating than inner ones that will maintain a more ordered SiO_4 tetrahedral group in structure during dehydroxylation. After heating at 950 °C, the SiO_4 groups combine with AlO_6 group to form the Al–Si spinel phase that in a short range order structure.

The Al–Si spinel phase appears at 920 °C and persists until at least 1150 °C. Brindley and Nakahira [3–5] suggested that the Al–Si spinel phase was produced by a topotatic transformation of metakaolinite because of the concomitant existence of the Al–Si spinel phase with metakaolinite at 920 °C. By the ED pattern analysis, the Al–Si spinel phase sat on metakaolinite and had lower symmetry with a rotation-related domain structure.[10] Mullite formed at 1000 °C and bearing crystallographic relation of Al–Si spinel phase and metakaolinite, resulting that *c* axis of mullite crystal is parallel to the <110> orientation of the Al–Si spinel phase, while the Al–Si spinel phase required the collapse of the metakaolinite structure. The mullite growth is accelerated by instantaneous nucleation process and the short distance diffusion. The mullite formation increases with the heating temperature increasing from 1050 to 1300 °C as shown in Fig. 1 (d) and (e), which also corresponds to the report of Chen et al.[19] Chakraborty and Ghosh[20] gave a reexamination of the Kaolin-mullite reaction series and more similar results have been provided.

3.2. Microstructure of mullite phase in kaolin

Fig. 2 shows the TEM microstructure and SAED patterns of kaolin sample sintered at 1300 °C for 30 min. Fig. 2(a) is the bright-field TEM image, showing a broad size distribution about 20–70 nm in width and 20–200 nm in length of mullite crystals which are embedded in the amorphous glassy phase. The initial mullite crystals show plate-like morphology. The chemical composition of various mullite crystals with different particle sizes of 20–70 nm, in Fig. 2 (M1–M5), was determined by TEM–EDS. The Al_2O_3 content in mullite crystal increases from 49.57 to 71.37 wt.% with the grain width increasing from 20 to 70 nm, and the chemical composition tends to be a stable 3/2 mullite ($3Al_2O_3{\cdot}2SiO_2$, 71.79 wt.% Al_2O_3) when the grain width grows up to 50 nm as listed in Table 2.

Two SAED patterns for M1 and M4 locations [in Fig. 2(a)] are shown in Fig. 2(b) and (c). The mullite

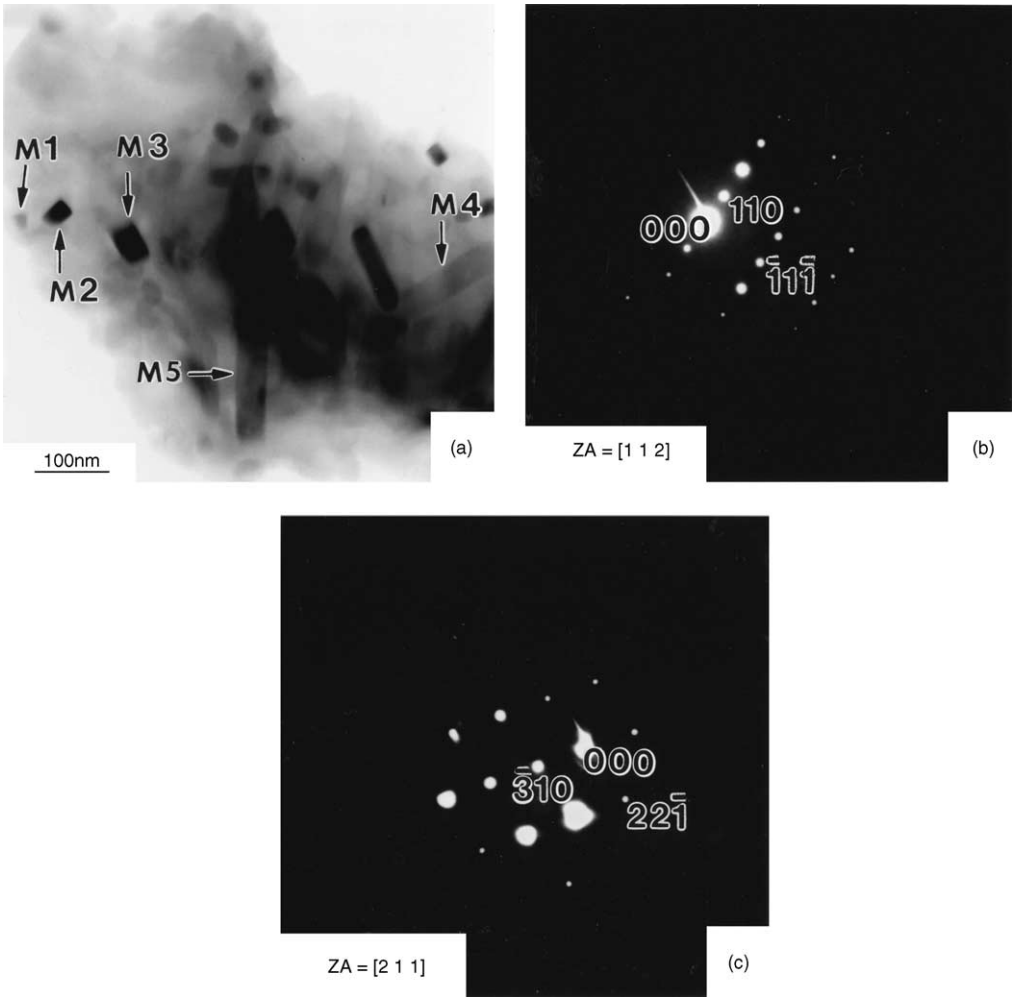

Fig. 2. TEM microstructure and SAED patterns of kaolin ceramics sintered at 1300 °C for 30 min for (a) bright field SAED pattern at; (b) M1 and (c) M4.

crystals identified by SAED patterns show that there are various crystallographic orientations indicating that mullite initially transformed from the less ordered kaolinite phase. All of these mullite crystals in Fig. 2(a) (M1–M5) show the orthorhombic structure with various lattice parameters. The mullite lattice parameters of *a*, *b* and *c* axis which were determined from the SAED patterns decrease from 8.085, 8.106 and 3.215 to 7.882, 7.974 and 2.976 Å, respectively, with the grain width increasing from 20 to 70 nm as shown in Fig. 3. According to Table 2, Figs. 2 and 3, the SiO_2 liberation from the initial mullite crystals during grain growth is demonstrated.

In the previous study, by maintaining the topotatic relationship between phases and according to the reaction model of Brindley and Nakahira,[4,5] proposed for the kaolinite–mullite transformation, the amorphous SiO_2 should be liberated gradually when the metakaolinite transforms to Al–Si spinel phase and mullite. Sanze et al. [21] exposed a natural kaolinite to DTA heating and applied the ^{27}Al and ^{29}Si MAS–NMR in a study of the kaolinite–mullite transformation, they found that aluminum is presented in *tetra*- and *penta*-coordinations of metakaolinite. Its tetrahedral sheet breaks down and changes the Al to more stable octahedral coordination.

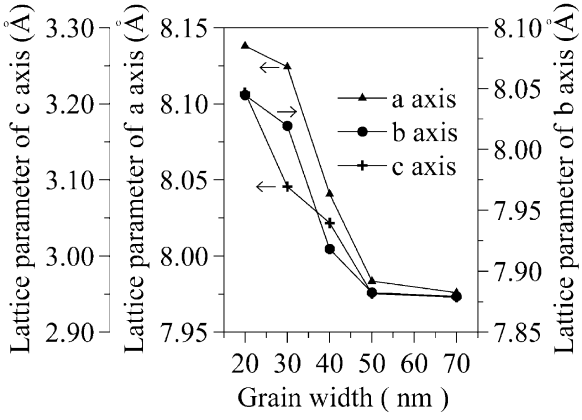

Fig. 3. Relation between mullite lattice parameters and grain width as kaolin ceramics sintered at 1300 °C for 30 min.

Table 2
The grain width and composition of mullite crystal by TEM–EDS analysis in Fig. 2(a)

Mark	Grain width (nm)	Composition (wt.%)	
		Al_2O_3	SiO_2
M1	20	49.57	50.43
M2	30	61.73	38.27
M3	40	65.40	34.60
M4	50	70.96	29.04
M5	70	71.37	28.63
3/2 mullite		71.79	28.21

After transformation, structural SiO_2 was released and all spectra show a poor crystal characteristic of Al–Si spinel and mullite phases.

3.3. Crystallization kinetics of mullite phase formation in kaolin

Fig. 4(a) shows the DTA/TG curves recorded during heating from 27 to 1400 °C of the kaolin at a heating rate of 10 °C min^{-1} in static air. The DTA curve shows two endothermic peaks at 110 and 530 °C and an exothermic one at 1006.5 °C. In TG trace, a two-step weight loss is observed. The weight loss of the first step at 110 °C is about 1.0 wt.%, corresponding entirely to the first endothermic peak in DTA; the weight loss of the second step as the heating temperature at 450–850 °C is around 7.7 wt.%, correlating with the second endothermic effect at 530 °C. On the other hand, the weight loss does not change significantly during the heating temperature at above 850 °C. The result shows that the first endothermic reaction is the evaporation of adsorbed water and the second endothermic event is the dehydration of kaolin. On the other hand, according to Fig. 1, the exothermic event at 1006.5 °C is irrefutable evidence for the mullite formation. In a reexamination of the kaolinite-to-mullite reaction series by Chakraborty and Ghosh,[20] the exothermic peak was given at 980 °C. This temperature (at 26 °C lower) might have been due to a different kaolinite sample having somewhat different impurities or particle size distribution of the starting material. An enlarge view of the exothermic peak ($T_{c,m}$) is shown in Fig. 4(b).

Fig. 5 reveals the DTA curves for kaolin ceramics with different heating rates. The $T_{c,m}$ position shifts to a higher temperature of 1022.6 °C as the heating rate increased to 40 °C min^{-1}. Technique of DTA has been extensively employed to investigate the thermal behavior of various materials. For phase transformation of various materials, it is especially important that in determining the transformation temperature, DTA technique was always employed.[22,23] The crystallization kinetics of the mullite formation in kaolin ceramics was

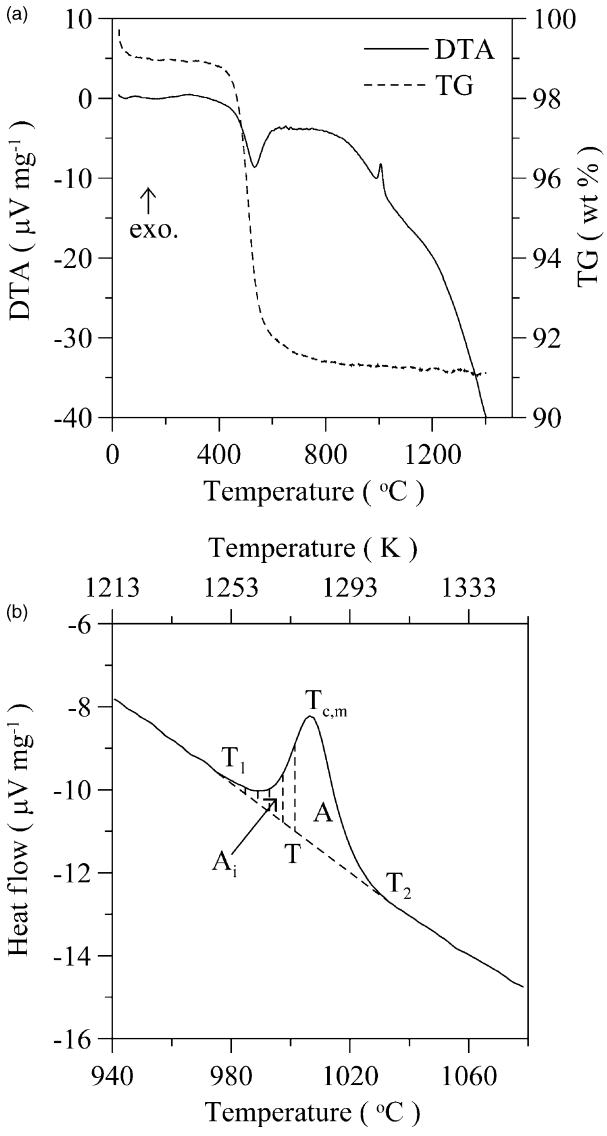

Fig. 4. (a) DTA/TG and (b) enlarged view of DTA curve of kaolin ceramics obtained at a heating rate of 10 °C min^{-1}.

also determined by DTA analysis.[14,16] Since the heat evolved in a small time interval is directly proportional to the number of moles reacting during that, the A_i [shown in Fig. 4(b)] deflection from the base line at any given instant is proportional to the instantaneous reaction rate.[24] The temperature, $T_{c,m}$ is dependent on the heating rate of β. Taking into account the $T_{c,m}$ temperature for Arrhenius type equation:[25]

$$\beta = CM \exp\left(-\frac{E_{c,m}}{RT_{c,m}}\right), \quad (4)$$

where $E_{c,m}$ is the activation energy for mullitization in kaolin, R denotes the gas constant, M means the number of nuclei, and C is a constant.

The following equation can be derived from the Johnson–Mehl–Avrami (JMA) equation:[26]

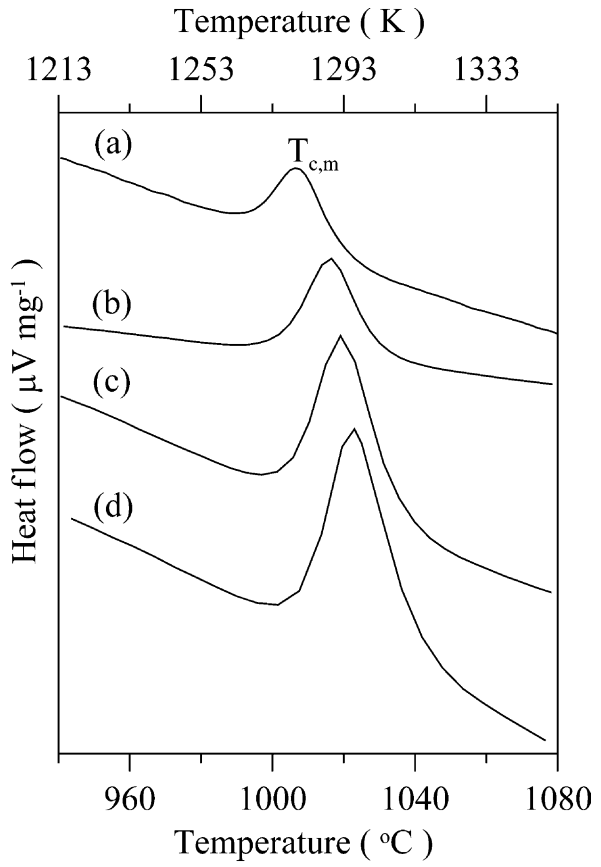

Fig. 5. The exothermic peak of the DTA curves for kaolin ceramics at various heating rates of (a) 10, (b) 20, (c) 30 and (d) 40 °C min^{-1}.

$$\ln\ \beta = -\frac{E_{c,\ m}}{RT_{c,\ m}} + \ln\ CM \tag{5}$$

where CM is a constant.

Fig. 6 illustrates the linear relationship between ln β and $\frac{1}{T_{c,m}}$, and the apparent activation energy of mullite formation in kaolin is calculated from the slope as 1182.3 kJ mol^{-1}. The mullite formation from the various raw materials and manufacture processes is directly depending on the chemical homogeneity of the components. It can be seen that the present value is higher than that of the kaolinite materials[8,17] and various Al_2O_3–SiO_2 precursors.[14–16,27]

When the kaolin sample is heated at a constant rate, $\frac{dT}{dt} = \beta$, the total number, N, of the mullite nuclei formed per unit volume, and the radius, r, of the mullite particle in the course of heating from room temperature (T_r) to T is expressed, respectively.[28–31]

$$N = \frac{1}{\beta}\int_{T_r}^{T} I(T)\mathrm{d}T = \frac{N_o}{\beta} \tag{6}$$

$$r = \frac{1}{\beta}\int_{T_r}^{T} U(T)\mathrm{d}T \tag{7}$$

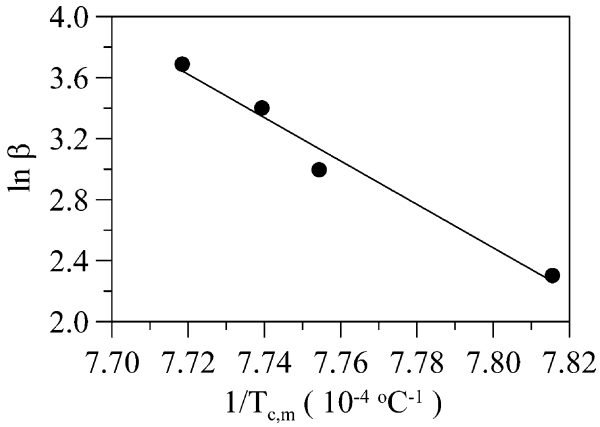

Fig. 6. Plots of ln β versus $1/T_{c,m}$.

where N_o denotes the initial number of nuclei, $I(T)$ and $U(T)$ are the rates of nucleation and crystal growth, respectively. $U(T)$ can be expressed as

$$U(T) = \nu_o\lambda\exp\left(-\frac{E_{m,g}}{RT}\right) = \mu\left(-\frac{E_{m,g}}{RT}\right), \tag{8}$$

where $E_{m,g}$ denotes the activation energy of mullite growth, and ν_o and λ are the frequency of a molecule tries to climb over an energy barrier, and thickness of one molecule layer of a phase, respectively.

The radius of the mullite particle, r, can be rewritten as[29,31–33]

$$r = \frac{1}{\beta}\int_{T_r}^{T} \mu_o\exp\left(-\frac{E_{m,g}}{RT}\right)\mathrm{d}T \approx \frac{r_o}{\beta}\exp\left(-\frac{E_{m,g}}{RT}\right), \tag{9}$$

where r_o denotes the initial length of the mullite particle.

There is only one type of mullite formation that takes place in kaolin, based on bulk nucleation. The volume fraction of the mullite crystal, α, in the bulk nucleation is expressed as:[32,33]

$$\frac{\mathrm{d}\alpha}{\mathrm{d}T} = \frac{4N_o r_o^{n-1}\mu_o}{\beta^n}(1-\alpha)\exp\left(-\frac{nE_{m,g}}{RT}\right), \tag{10}$$

where $\alpha = \frac{A_i}{A}$, A is the area under DTA curve between T_1, the temperature at which mullite formation starts; and T_2, the temperature at which mullite nucleation is completed, A_i is the area between T_1 and T as shown in Fig. 4(b).

Accordingly,

$$-\ln(1-\alpha) = \frac{K}{\beta^{n+1}}\ \exp\left(-\frac{nE_{m,g}}{RT}\right), \tag{11}$$

by using Eqs. (10) and (11), the following simplified expression is derived:

$$-\ln(1-\alpha) = \frac{K'}{\beta^m}\ \exp\left(-\frac{nE_{m,g}}{RT}\right), \tag{12}$$

that is,

$$\log[-1n(1-\alpha)] = -m \quad \log\beta - \frac{1}{2.303}\frac{nE_{m,g}}{RT} + \text{constant}, \tag{13}$$

where m and n denote the numerical values for various crystallization mechanisms. When a sample crystallizes during a DTA run, the heat of crystallization is evaluated and an exothermic peak is related to the growth morphology parameter, n, in which the higher the value of n the narrower the peak. The plots of log $[-\ln(1-\alpha)]$ against $\frac{1}{T}$ for kaolin samples obtained at various heating rates are shown in Fig. 7. The value of nE is obtained from the slopes of the straight lines and the n values can be obtained by dividing the nE values by the activation energy determined in Eq. (5). The values of n increase with heating rate increasing as listed in Table 3, and the DTA curve shows a narrower peak at a higher heating rate of 40 °C min^{-1} as shown in Fig. 5.

3.4. Growth mechanism of mullite formation in kaolin

Fig. 8 presents the value of growth morphology parameter n thus obtained as a function of heating rate. It is found that for kaolin sample, n is 2.0 at a heating rate of 10 °C min^{-1}, and increases gradually to 2.3 as the heating rate increases to 40 °C min^{-1}. Within experimental error, the average value is approximated as 2.0. The nonisothermal result with a reaction order n of 2.0 can be estimated. From JMA criterion, n of 2 describes two-dimensional growth from a constant number of nuclei and shows a plate-like morphology[34] that is observed by TEM [in Fig. 2(a)].

Fig. 9 reveals the plots of log $[-\ln(1-\alpha)]$ versus log β for mullite formation in kaolin at various temperatures.

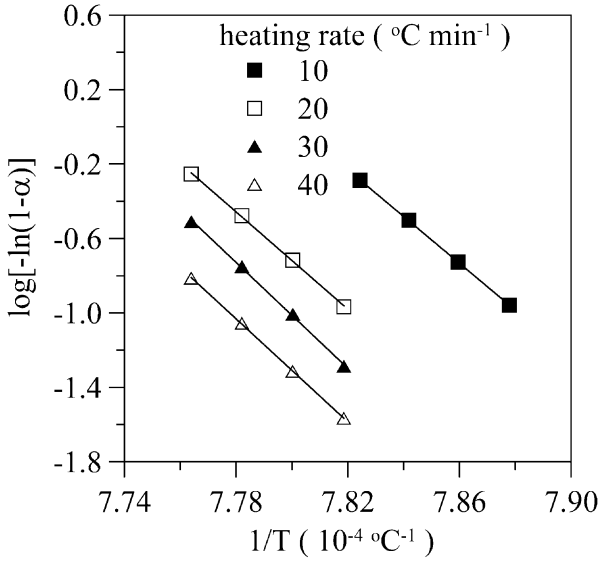

Fig. 7. Plots of log$[-\ln(1-\alpha)]$ versus $1/T$ at various heating rate.

Table 3
Growth morphology parameters of n and m at various heating rates and temperatures by using Eq. (13)

Heating rate (°C min^{-1})	nE (kJ mol^{-1})	n	m
10	2406.0	2.0	2.0
20	2500.8	2.1	2.0
30	2720.8	2.3	1.9
40	2649.0	2.3	1.8
Average	2569.2	2.2	1.9

According to Eq. (13), it is found that for mullite formation in kaolin, m is close to 2.0 at low temperatures of mullite formation and decreases to 1.8 when the mullite formation temperature increases. Within experimental error, these values are also approximated as 2.0. Results of Figs. 8 and 9 agree with the fact that n and m are both close to 2.0. These results also indicate that the bulk nucleation is dominant in mullite crystallization and the crystal growth is controlled by diffusion at a fixed number of nuclei in kaolin. It is further known that the contribution of bulk nucleation decreases with the heating rate increasing.

McConnell and Fleet[35] used the kaolin ceramics as the starting materials and fired at temperatures between 1150 and 1225 °C, obtaining more lathlike or rod shaped mullite crystals. It is found that the morphology of the original platelets is maintained until well after the dehydroxylation temperature. McConville et al.[9] also have obtained a similar result by firing kaolinite materials. On the other hand, Campos et al.[16] used the diphasic gel of aluminium–silicon xerogel and obtained the plate-like mullite crystal as sintered at 1350 °C. Wang[36] also pointed out that for both nonisothermal and isothermal treatments of the 65 wt.% Al_2O_3–35 wt.% SiO_2 glass fibers, the growth morphology parameter n of 2.0 shows a plate growth mode of mullite.

A similar behavior of the kaolinite–mullite reaction kinetics has been experimentally obtained by Gualtieri

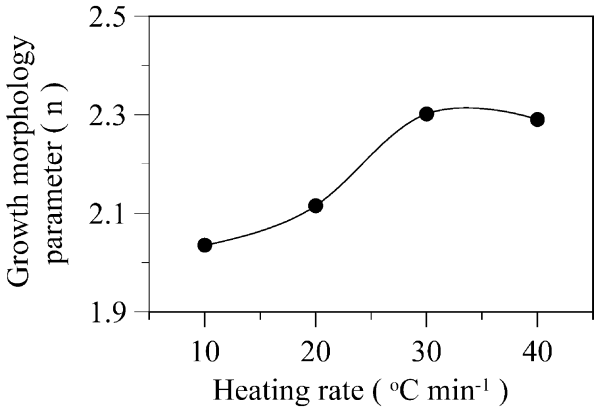

Fig. 8. Variation of growth morphology parameter n with heating rate.

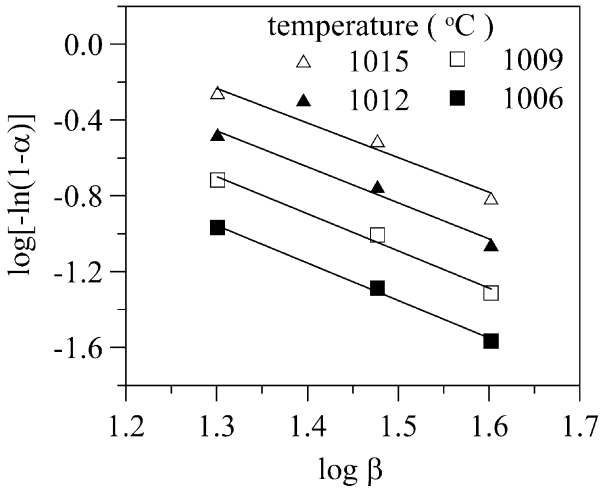

Fig. 9. Relation between log[−ln(1−α)] versus log β at various temperatures for kaolin ceramics.

et al.,[8] in which the initial reaction mechanism was characterized by instantaneous mullite nucleation. And the lower order of the reaction indicates that the chemical diffusion plays a non-negligible role in mullite crystallization. The mechanism through which mullite crystallizes is also dependent on the homogeneity of the precursor raw materials. The kinetics parameters of mullite crystallization from a diphasic gel have been measured using a non-isothermal method,[16] indicating that the rate controlled step may be the short distance diffusion of alumina and silica along the mullite grain boundaries.

4. Conclusion

The crystallization kinetics and growth mechanism of mullite formation in kaolin ceramics were investigated using XRD, TEM, SAED, EDS and DTA. The results of this study are summarized as follows:

1. The mullite which is transformed from kaolin appears at 1050 °C by XRD and tallies with DTA.
2. As the Al_2O_3 content in mullite crystal increases from 49.57 to 71.37 wt.%, the lattice parameters of *a*, *b* and *c* axis decrease from 8.085, 8.106 and 3.215 to 7.882, 7.974 and 2.976 Å, respectively, while the mullite grain width increases from 20 to 70 nm.
3. The nonisothermal activation energy of mullite crystallization in kaolin is 1182.3 kJ mol^{-1}.
4. The value of growth morphology parameter *n* increases from 2.0 to 2.3 but *m* decreases from 2.0 to 1.8 with the heating rate increasing from 10 to 40 °C min^{-1}. Within experimental error, the values of *n* and *m* are both approximated as 2.0, indicating two-dimensional growth from a constant number of nuclei and resulting in a plate-like morphology.

Acknowledgements

The financial support from the National Science Council of Taiwan, ROC, for grant No. 89-2216-E-006-072 is appreciated. The authors sincerely thank Professor F.S. Yen for the DTA analysis and Mr. H.Y. Yao for the TEM–EDS analysis.

References

1. Gruner, J. W., The crystal structure of kaolinite. *Z. Kristallogr.*, 1932, **83**, 75–80.
2. Freimann, S. and Rahman, S., Refienement of the real structures of 2:1 and 3:2 mullite. *J. Eur. Ceram. Soc.*, 2001, **21**, 2453–2461.
3. Brindley, G. W. and Nakahira, M., The kaolinite–mullite reaction series: I. A survey of outstanding problems. *J. Am. Ceram. Soc.*, 1959, **42**, 311–314.
4. Brindley, G. W. and Nakahira, M., The kaolinite–mullite reaction series: II. Metakaolin. *J. Am. Ceram. Soc.*, 1959, **42**, 315–318.
5. Brindley, G. W. and Nakahira, M., The kaolinite–mullite reaction series: III. The high temperature phases. *J. Am. Ceram. Soc.*, 1959, **42**, 319–324.
6. Guse, W. and Mateika, D., Growth of mullite single crystals ($2Al_2O_3{\cdot}SiO_2$) by the Czochralski method. *J. Cryst. Growth*, 1974, **22**, 237–240.
7. Guse, W., Composition analysis of Czochralski grown mullite single crystals. *J. Cryst. Growth*, 1974, **26**, 151–152.
8. Gualtieri, A., Bellotto, M., Artioli, G. and Clark, S. M., Kinetic study of the kaolinite–mullite reaction sequence. Part II: mullite formation. *Phys. Chem. Minerials*, 1995, **22**, 215–222.
9. McConville, C. J., Lee, W. E. and Sharp, J. H., Sharp, Microstructural evolution in fired kaolinite. *Br. Ceram. Tran.*, 1998, **97**, 162–168.
10. Lee, S., Kim, Y. J. and Moon, H. S., Phase transformation sequence from kaolinite to mullite investigated by an energy-filtering transmission electron microscope. *J. Am. Ceram. Soc.*, 1999, **82**, 2841–2848.
11. Castelein, O., Guinebretière, R., Bonnet, J. P. and Blanchart, P., Shape, size and composition of mullite nanocrystals from a rapidly sintered kaolin. *J. Eur. Ceram. Soc.*, 2001, **21**, 2369–2376.
12. Pask, J. A. and Tomsia, A. P., Formation of mullite form sol-gel mixtures and kaolinite. *J. Am. Ceram. Soc.*, 1991, **74**, 2367–2373.
13. Pehak, P., Kunath-Fandrei, G., Losso, P., Hildmann, B., Schneider, H. and Jäger, C., Study of the Al coordination in mullites with varing Al:Si ratio by 27Al NMR spectroscopy and X-ray diffraction. *Am. Miner.*, 1998, **83**, 1266–1276.
14. Boccaccini, A. R., Khalil, T. K. and Bücker, M., Activation energy for the mullitization of a diphasic gel obtained from fumed silica and boehmite sol. *Mater. Lett.*, 1999, **38**, 116–120.
15. Holm, J. L., Kaolinites–mullite transformation in different Al_2O_3–SiO_2 systems: thermo-analytical studies. *Phys. Chem. Chem. Phys.*, 2001, **3**, 1362–1365.
16. Campos, A. L., Silva, N. T., Melo, F. C. L. and Oliveria, M. A. S., Crystallization kinetics of orthorhombic mullite from diphasic gels. *J. Non-Cryst. Solids*, 2002, **304**, 19–24.
17. Castelein, O., Soulestin, B., Bonnet, J. P. and Blanchart, P., The influence of heating rate on the thermal behaviour and mullite

formation from a kaolin raw material. *Ceram. Int*., 2001, **27**, 517–522.
18. Li, D. X. and Thomson, W. J., Tetragonal to orthorhombic transformation during mullite formation. *J. Mater. Res*., 1991, **6**, 819–824.
19. Chen, Y. F., Wang, M. C. and Hon, M. H., Pore structure and properties of kaolin-silica-alumina ceramics. *J. Ceram. Soc. Jpn*., 2003, **111**, 537–543.
20. Chakraborty, A. K. and Ghosh, D. K., Reexamination of the kolinite-to-mullite reaction series. *J. Am. Ceram. Soc*., 1978, **61**, 170–173.
21. Sanz, J., Madani, A., Serratosa, J. M., Moya, J. S. and Aza, S., Aluminum-27 silicon-29 magic-angle spinning nuclear magnetic resonance study of the kaolinite–mullite transformation. *J. Am. Ceram. Soc*., 1988, **71**, c418–c421.
22. Yen, F. S., Wang, M. Y. and Chang, J. L., Temperature reduction of θ- to α-phase transformation induced by high-pressure pretreatments of nano-sized alumina powders derived from boehmite. *J. Cryst. Growth*, 2002, **236**, 197–209.
23. Yen, F. S., Chang, J. L. and Yu, P. C., Relationships between DTA and DIL characteristics of nano-sized alumina powder during θ- to α-phase tansformation. *J. Cryst. Growth*, 2002, **246**, 90–98.
24. Borchardt, H. J. and Danields, F., The application of differential thermal analysis to the study of reaction kinetics. *J. Am. Chem. Soc*., 1957, **79**, 41–46.
25. Marotta, A., Buri, A. and Valent, G. L., Crystallization kinetics of gehlenite glass. *J. Mater. Sci*., 1978, **13**, 2483–2486.
26. Marotta, A. and Buri, A., Kinetics of devitrification and differential thermal analysis. *Therm. Acta*, 1978, **25**, 155–160.
27. Chen, Y. F., Wang, M. C. and Hon, M. H., Transformation kinetic and mechanism of kaolin–Al_2O_3 ceramics. *J. Mater. Res*., 2003, **18**, 1355–1362.
28. Matusita, K., Sakka, S., Maki, T. and Tashiro, M., Study on crystallization of glass by differential thermal analysis. Effect of added oxide on crystallization of LiO_2–SiO_2 glasses. *J. Mater. Sci*., 1975, **10**, 94–100.
29. Matusita, K. and Sakka, S., Kinetic study of the crystallization of glass by differential scanning calorimetry. *Phys. Chem. Glasses*, 1979, **20**, 81–84.
30. Matusita, K. and Tashiro, M., Rate of homogeneous nucleation in alkali disilicate glasses. *J. Non-Cryst. Solids*, 1973, **11**, 471–484.
31. Matusita, K., Maki, T. and Tashiro, M., Effect of added oxides on the crystallization and phase separation of Li_2O–$3SiO_2$ glasses. *Phys. Chem. Glasses*, 1974, **15**, 106–108.
32. Matusita, K., Sakka, S. and Matsui, Y., Determination of the activation energy for crystal growth by differential thermal analysis. *J. Mater. Sci*., 1975, **10**, 961–966.
33. Matusita, K. and Tashiro, M., Effect of added oxides on the crystallization of Li_2O–$2SiO_2$ glasses. *Phys. Chem. Glasses*, 1973, **14**, 77–80.
34. Hsi, C. S. and Wang, M. C., Crystallization kinetics and phase transformation of Li_2O–Fe_2O_3–MnO_2–CaO–P_2O_5–SiO_2 glass. *J. Mater. Res*., 1998, **13**, 2655–2661.
35. McConnell, J. D. C. and Fleet, S. G., Electron optical study of the thermal decomposition of kaolinite. *Clay Miner*., 1970, **8**, 279–290.
36. Wang, M. C., Thermal determinations of mullite crystallization of 65% Al_2O_3–35% SiO_2 glass fibers. *Chinese J. Mater. Sci*., 1992, **24**, 164–170.